SIMULATION OF SIMULTANEOUS HEAT AND MOISTURE TRANSFER BY USING THE FINITE DIFFERENCE METHOD AND VERIFIED TESTS IN A TEST CHAMBER

S.P.W. Wong
Fellow ASHRAE

ABSTRACT

In this paper, a series of tests were performed in a test chamber to investigate the parameters and the rate of the simultaneous heat and moisture transfer between the building envelope and space air during the operating period and the off-period. Prior to the tests, many preliminary tests also had been performed to determine the characteristics of the test chamber as well as the repeatability of the thermocouples.

Simulation of the simultaneous heat and moisture transfer in the same test chamber by using the finite difference method was performed and analyzed with the aid of a microcomputer. The mathematical models of heat and moisture balance at various nodes of the building structure were introduced and discussed.

Finally, the simulated values were compared against the actual measured values of the tests. The operating characteristics of the test chamber were analyzed and the influence of the variation of the convective heat transfer coefficient, the coefficient of structural characteristics, and the radiative energy was discussed.

INTRODUCTION

In another paper by the authors entitled, "Fundamentals of Simultaneous Heat and Moisture Transfer between the Building Envelope and the Conditioned Space Air," theories and models of simultaneous heat and moisture transfer between the building envelope and the conditioned space air under intermittent operation of an air system were discussed. The finite difference method was used to solve such a mathematic model. In this paper:

1. Tests of simultaneous heat and moisture transfer between the building envelope and space air at various supply volume flow rates of conditioned air took place in a test chamber.
2. System simulations of simultaneous heat and moisture transfer during the operating period and the off-period using the finite difference method in the same test chamber were analyzed and carried out with the aid of a microcomputer.
3. Calculated results of simultaneous heat and moisture transfer from system simulation were compared against the actual measured readings from the test.

Construction of the Test Chamber and the Measuring Instruments

The test chamber, shown in Figure 1, is 2.78 m (9.12 ft) wide by 3.6 m (11.18 ft) long, for an area of 10 m² (107.6 ft²).

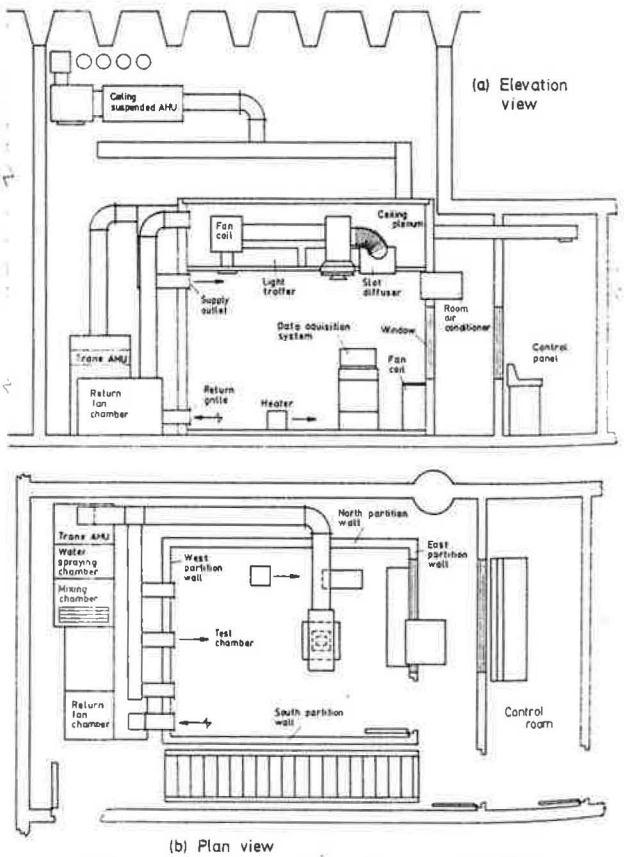

Figure 1 *Construction of the test chamber*

S.P.W. Wong is Managing Partner, Associated Consulting Engineers, Hong Kong.

The height from the floor to the ceiling is 2.32 m (7.61 ft). The east side of the chamber has a window 1 m (3.28 ft) high by 1.4 m (4.59 ft) wide so that tests can be seen from the buffer zone of the chamber. An independent air handler was installed adjacent to the west side of the test chamber in order to maintain the required temperature and relative humidity inside the chamber. This air handler is composed of: a supply fan, a cooling coil, a water spraying chamber, an electric heater, and a mixing chamber with viscous and reusable low-efficiency air filters. An additional return fan is mounted in a return fan box. Both supply and return fans are driven by variable-speed motors, each employing an eddy current clutch.

Conditioned air from the air handler was supplied from the high-side wall outlets. Space air was returned from the low-level return grilles.

The partition walls forming the four sides of the test chamber are composed of an outer layer of 18 mm (0.71 in.) thick plywood panel, an air gap which has a passage connecting to the ceiling plenum, and an inside layer of acoustic tile of mineral fiber with a thickness of 18 mm (0.71 in.). The ceiling is also made from 18 mm (0.71 in.) acoustic tile. Hardwood floors of 24 mm (0.95 in.) thickness are directly mounted on the concrete slab. The east-side window is of single-glazed clear plate with a thickness of 5.4 mm (0.2 in.). The wooden door is also made from plywood having an air space between the two plywood panels.

The entire chamber is surrounded by a constant-temperature buffer zone except the space beneath the floor. A separate ceiling-suspended air handler is installed to maintain the required temperature in the buffer zone. Outside the east buffer zone, there is a control room. The speed of the supply and return fan motor can be modulated at the control panel mounted on a table.

The measuring instruments used in the tests include: a data acquisition/microcomputer control unit, a hot-wire-type anemometer, a set of pitot-static tubes and a manometer, two aspiration psychrometers, and 21 copper-constantan thermocouples.

Preliminary Tests

Tests of heat and moisture transfer in the test chamber can be classified into two categories: preliminary tests and principal tests.

Preliminary tests took place prior to the principal tests for the sake of investigating the repeatability of the thermocouples and other parameters in the test chamber.

Investigation of Thermocouples All 21 hot junctions of copper-constantan thermocouples were held together to sense the same localized air temperature in the test chamber. The conditioned air is supplied at a volume flow rate of 133 L/s (282 cfm). The purpose of the investigation was to select the thermocouples that will measure air or surface temperature at a resolution of 0.1°C (0.18°F) with satisfactory repeatability. Most readings had only a maximum variation of 0.2°C (0.36°F) between various thermocouples in the same scanning during the investigation.

Measuring of the Supply Volume Flow Rates The supply volume flow rates were measured at the high-side wall circular outlet prior to the principal tests. The motor speeds of the supply fan were fixed at 200 rpm, 405 rpm, 650 rpm, and 805 rpm, respectively, during these measurements. The return fan was not operating. For each motor speed, 24 measuring points based on the equal area principle were located at the circular outlet. A pitot tube and an inclined manometer were then used to measure the velocity pressure of the supply air at the outlet. Supply air velocity and the supply volume flow rate were then calculated. The results of these measurements are shown in Table 1.

TABLE 1 Measurements of the Supply Flow Rates

Motor speed rpm	Supply fan speed rpm	Average supply velocity, m/s (fpm)	Supply volume flow rate L/s (cfm)
200	540	4.33 (852)	41.2 (87)
405	1094	9.13 (1797)	81.4 (172)
650	1755	14.0 (2755)	133.2 (282)
805	2175	18.0 (3542)	171.1 (362)

Mean Air Velocity Flowing Over the Building Envelope For the purpose of calculating the mean convective heat transfer coefficient, the velocity of the airstream flowing over the building envelope at various speeds of the supply fan was measured. Usually, nine points were measured for each surface of a building structure.

Air Temperature Distribution and Gradients In order to find a point on the surface of the building envelope to represent approximately the average temperature of the surface, the surface temperature distribution of various building structures was measured. During these measurements, the conditioned air was supplied at a volume flow rate of 133 L/s (282 cfm). For each surface of the building envelope, at least nine readings were measured.

Figure 2 shows the dry-bulb, wet-bulb, and humidity ratio distribution of the space air in the test chamber measured on April 26, 1988, when the supply volume flow rate was 133 L/s (282 cfm). In Figure 2, the vertical gradients of the dry-bulb, wet-bulb, and humidity ratio are obvious. Air temperatures are higher at the west end of the chamber compared to the east end.

The vertical gradients of the dry-bulb, wet-bulb, and humidity ratio of the space air at the center of the test chamber are smallest compared with other locations due to greater air circulation.

Types of Surface Contact By using thermocouples to measure the surface temperature of the building envelope, three types of contact between the hot junction and the surface had been investigated at a supply volume flow rate of 133 L/s (282 cfm):

1. The copper and constantan wires were soldered to the upper part of a 100 mm² (0.16 in.²) copper plate with

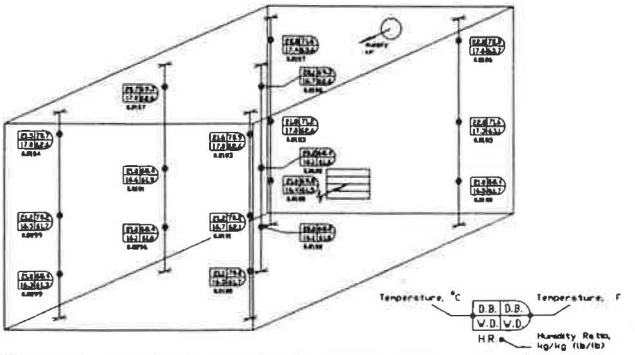

Figure 2 Dry-bulb, wet-bulb, and humidity ratio distribution in the test chamber when the supply flow rate is 133 L/s (282 cfm)

TABLE 2
Verification of Moisture Gain from Building Envelope

Supply Air				Return Air						
Time	Dry Bulb °C (°F)	Wet Bulb °C (°F)	Humidity Ratio kg/kg (lb/lb)	Time	Dry Bulb °C (°F)	Wet Bulb °C(°F)	Humidity Ratio kg/kg (lb/lb)	Humidity Ratio W kg/kg (lb/lb)	Total Latent Load W(Btu/h)	Moisture Gain from Building Envelope W (Btu/h)
9.24	16.0 (60.8)	14.4 (57.9)	0.0097	9.27	20.0 (68)	16.8 (62.2)	0.0108	0.0011		
9.31	15.5 (60)	14.2 (57.6)	0.00965	9.34	20.4 (68.7)	16.8 (62.2)	0.0106	0.00095		
9.39	15.5 (60)	14.2 (57.6)	0.00965	9.41	20.0 (68)	16.5 (61.7)	0.0106	0.00095		
9.50	15.5 (60)	14.3 (57.7)	0.00975	9.54	20.0 (68)	16.5 (61.7)	0.0106	0.00085		
10.10	15.8 (60.4)	14.6 (58.3)	0.0099	10.15	20.0 (68)	16.6 (61.9)	0.0107	0.0008	406	
							Average	0.00093	(1386)	306 (1044)

a thickness of about 0.5 mm (0.2 in.). The bottom part of the copper plate was taped firmly to the surface. The measured temperature difference between the surface of the partition and the adjacent air was about 0.1°C (0.18°F).

2. The twisted hot junction of copper-constantan wire was stuck on the surface of the partition by a piece of tape. The measured temperature difference is slightly less than 0.2°C (0.36°F).

3. The twisted hot junction was stuck on the surface by a piece of foam-like tape about 3 mm (0.12 in.) thick. The measured temperature difference is about 0.2°C (0.36°F).

In order to avoid the influence of ambient air during the surface temperature measurement, the third type of surface contact was adopted.

Verification of Moisture Gain from Building Envelope in the Test Chamber On May 3, 1988, the dry- and wet-bulb temperatures of the supply and return air were measured by the same aspiration psychrometer during consecutive measurements. The motor speed of the supply fan was 700 rpm and the measured supply flow rate was 145 L/s (307 cfm). The results are listed in Table 2.

There were two occupants in this chamber during this test. The latent load for each occupant at light work at a temperature of 20°C (68°F) is about 50 W (171 Btu/h). Hence, the average moisture gain from building envelopes, in terms of latent load between 9:24 a.m. and 10:15 a.m., was about 306 W (1044 Btu/h).

Air Infiltration Air pressure inside the test chamber was measured at a value of about 0.5 Pa (0.002 in. water column) higher than the surrounding buffer zones at a supply flow rate of 133 L/s (282 cfm). Airflow direction showed that air exfiltrated from the gap of the partition wall to the surrounding buffer zones.

PRINCIPAL TESTS

Principal tests consist of the tests of heat and moisture transfer and space operating characteristics of the test chamber. A series of four tests at various supply flow rates had been completed consecutively, as shown in Table 3.

In each test, 21 channels of thermocouple readings were scanned once every 10 minutes by the data acquisition unit. For a 24-hour operating cycle, there were 144 scans altogether. Table 4 shows a typical scan at 9:56 a.m. on June 28, 1988, during the operating period of Test 1.

The distance between the hot junction of the thermocouple to measure the air temperature adjacent to the surface and the surface is about 25 mm (1 in.), which is greater than the thickness of the laminar boundary layer flowing over the surface of the building envelope.

Two operators were allowed to enter this chamber before the air handler and the electric lighting were switched on in order to add water to the wet-bulb cups and to set the computer program to scan the thermocouples during the operating period. The time duration was always less than 10 minutes. After the air handler and electric lighting were switched off, one operator was allowed to enter the chamber to set the control program of the data acquisition unit for nighttime operation.

Altogether there were 16 fluorescent tubes in four light troffers. Each of the fluorescent tubes has an input wattage of 65 W (222 Btu/h). The rated wattage for the data acquisition system was 190 W (648 Btu/h), and the heat released was about $190 \times 0.85 \times 0.1 = 16$ W.

A warm air electric heater was adjusted against a multimeter at an input wattage of 300 W (1024 Btu/h). It was then placed in the test chamber to be used as a space sensible load.

TABLE 3
Description of Principal Tests

Test	Time Duration	Air Handler, Electric Lighting and Heater		Motor Spaced of Supply Fan rpm	Supply Volume Flow Rate V_s, L/s (cfm)
		Switched On	Switched Off		
	June 27 to July 1, 1988				
1	27, 9:00 am to 28, 8:40 am	27, 9:23 am	27, 16:50 pm	650	133 (282)
2	28, 8:42 am to 29, 8:36 am	28, 8:54 am	28, 16:54 pm	650	133 (282)
3	29, 8:37 am to 30, 8:30 am	29, 16:48 pm	29, 16:48 pm	405	81.4 (172)
4	30, 8:31 am to July 1, 8:30 am	30, 8:58 am	30, 16:48 pm	200	41.2 (87)
5	July 1, 8:31 am to July 1, 16:00 pm	July 1, 8:58 am	July 1, 16:00 pm	805	171.1 (362)

TABLE 4
Typical Scan of the Temperature Reading of 21 Channels, June 28, 1988, 9:56 am

EXP C1—SCAN 08	07:28 : 9:56 : 00	
...00	21.5 °C	Air temperature in the air gap
...01	17.2 °C	Dry-bulb of the supply air
...02	15.6 °C	Wet-bulb of the supply air
...03	20.6 °C	Dry-bulb of the return air
...04	17.7 °C	Wet-bulb of air temperature adjacent to 10
...05	21.4 °C	Inner part of floor temperature
...06	21.3 °C	Surface temperature of east partition wall
...07	21.3 °C	Inner temperature of east partition wall
...08	21.1 °C	Dry-bulb of air temperature adjacent to 06
...09	17.4 °C	Wet-bulb of air temperature adjacent to 06
...10	21.2 °C	Surface temperature of the floor
...11	21.0 °C	Dry-bulb of air temperature adjacent to 10
...12	17.2 °C	Wet-bulb of the return air
...13	24.7 °C	Surface temperature of the plexiglass of the light troffer
...14	21.0 °C	Surface temperature of the suspended ceiling
...20	20.7 °C	Dry-bulb of the air temperature inside the ceiling
...21	17.5 °C	Wet-bulb of the air temperature inside the ceiling
...22	20.8 °C	Inner surface temperature of the window glass
...23	21.8 °C	Air temperature above the ceiling plenum
...24	21.0 °C	Air temperature in the corridor
...25	32.4 °C	Surface temperature of the light troffer inside the ceiling plenum

The air handler, electric lighting, and heater were switched on and off at the same time. Only the data acquisition system was operated continuously during the testing period.

Simulation of Simultaneous Heat and Moisture Transfer in the Test Chamber Using the Finite Difference Method

During the simulation of the simultaneous heat and moisture transfer process in the test chamber, as shown in Figure 1, the following assumptions are made in order to simplify the problem:

1. Consider a one-dimensional transient heat and moisture transfer only.
2. Building materials are homogeneous.
3. The heat and mass transfer coefficients are constants.
4. The airstream properties flowing over the surface of the building envelope are homogeneous.
5. Heat and moisture transfer at the corners of the test chamber are small and negligible.
6. The surface temperature difference between the building structures is small; therefore, the radiative exchange between these surfaces, except between the surface of the light troffer and the surfaces of the building envelope, is neglected.

Finite Difference Method

The finite difference method divides the building envelope into a number of sections. A fictitious node is located at the center of each section or on the surface of the surface section, as shown in Figure 3. An energy or mass balance occurring on the node results in an algebraic equation to solve the temperature or moisture content of this node in terms of the neighboring nodal temperatures or moisture contents, also in terms of the geometry, and the thermal and hygro-properties of the building material.

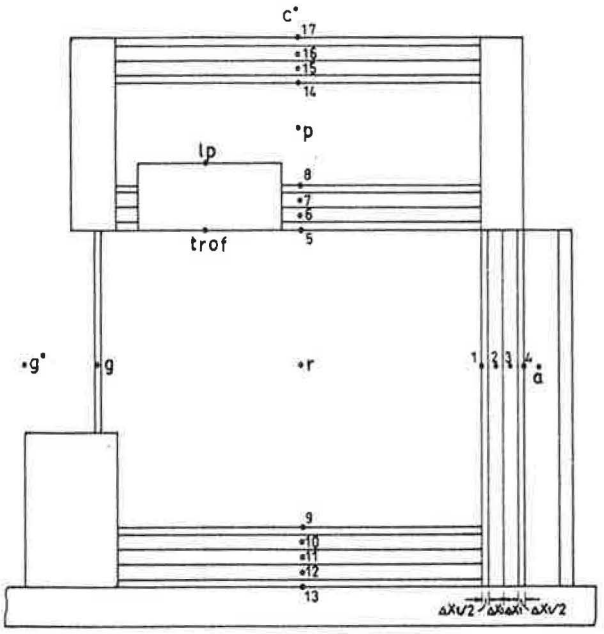

Figure 3 *Nodes of the test chamber*

Heat conduction can be approximated by the finite-difference form of the Fourier law:

$$q_{(i+1)\_i} \cong kA\frac{T_{(i+1)}^{t} - T_i^{t}}{\Delta x} \tag{1}$$

In Equation 1, superscript t at the upper right corner indicates time t.

Each nodal equation is solved explicitly in terms of the future temperature of that node. The time derivative is then approximated by a forward finite difference in time:

$$\frac{\partial T_i}{\partial t} \cong \frac{T_i^{t+\Delta t} - T_i^{t}}{\Delta t} \tag{2}$$

The explicit finite difference method will be adopted here most of the time because of its clarity and simplicity.

Nodes of the Test Chamber

For each section, there is a numbered center node or surface node to represent it, as shown in Figure 3.

South, west, north, and east partition walls of the test chamber are all divided into four sections. Two of them are surface nodes 1 and 4, and the other two sections are interior nodes 2 and 3. For surface nodes, the width of the section is $\Delta x_1/2$, and for the interior nodes, the width of the section is Δx_1. The surface of node 1 is in contact with the space air, r, and the surface of node 4 is in contact with the air in the air gap, a, of the partition wall. The total surface area of node 1, that is, the surface area of the partition wall, is 26.5 m² (285 ft²).

The ceiling is made of the same acoustic tile as the partition wall and has the same thickness. The ceiling is also divided into four sections. The width of the sections is the same as in the partition wall. Since a part of the suspended ceiling is occupied by the recessed mounted light troffers, the area of the suspended ceiling is only 6.5 m² (70 ft²).

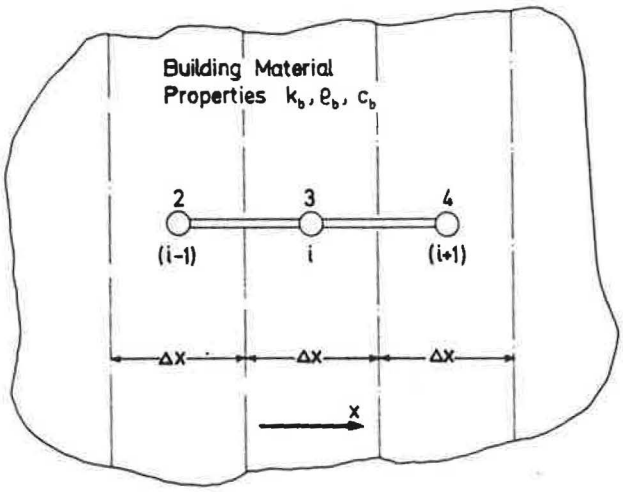

Figure 4 *Interior nodes in a one-dimensional heat and moisture transfer*

The wooden floor is divided into five sections. The node for the interface section contact with the concrete slab was 13. For simplicity, the area of the wooden door and the surface area of the wooden furniture are included in the floor, that is, a total area of 14 m² (151 ft²). Window glass is represented by an interior node, *g*.

The surface of the four bottom plexiglass plates of the light troffer is represented by a node, *trof*, and has a total surface of 3.5 m² (37.7 ft²). The surfaces of the upper part of the light troffer inside the ceiling plenum are represented by the node *lp* and have a total surface area of about 5.5 m² (59.2 ft²).

The upper and side panels of the ceiling plenum are all made of plywood panels of the same thickness. They are divided into four sections. The total area of these panels is about 25 m² (269 ft²).

Conditions of space air in the test chamber, plenum air, air above the ceiling plenum, and air outside the window glass are represented by the subscripts *r, p, o* and *og*, respectively.

Heat Transfer at the Interior Nodes

Consider interior node 3, as shown in Figures 3 and 4. For one-dimensional heat flow, if there is no internal energy generation, according to the first law of thermodynamics:

Conductive heat from node 2 + Conductive heat from node 4 = Rate of change of internal energy of node 3

$$q_{2\_3} + q_{4\_3} = \frac{\partial U_3}{\partial t} \tag{3}$$

and

$$\frac{\partial U_3}{\partial t} \cong \rho_b c_b A \Delta x \frac{T_3^{t+\Delta t} - T_3^t}{\Delta t} \tag{4}$$

Substituting Equations 1 and 4 into Equation 3,

$$k_b A \frac{T_2^t - T_3^t}{\Delta x} + k_b A \frac{T_4^t - T_3^t}{\Delta x} = \rho_b c_b A \Delta x \frac{T_3^{t+\Delta t} - T_3^t}{\Delta t}$$

Solving for the temperature for interior node 3 at time $t + \Delta t$:

$$T_3^{t+\Delta t} = \text{Fo}(T_2 + T_4) + (1 - 2\text{Fo})\, T_3 \tag{5}$$

In Equation 5, Fo is the Fourier number and is defined as

$$\text{Fo} = \frac{\alpha \Delta t}{(\Delta x)^2} = \frac{k_b}{\rho_b c_b} \frac{\Delta t}{(\Delta x)^2} \tag{6}$$

For an interior node, *i*, and two neighboring nodes $(i - 1)$ and $(i + 1)$, Equation 5 can be rewritten in the form

$$T_i^{t+\Delta t} = \text{Fo}\,(T_{(i-1)}^t + T_{(i+1)}^t) + (1 - \text{Fo})T_i^t \tag{7}$$

When Equation 7 is used to determine the temperature of node *i* at time $t + \Delta t$, the choice of spacing, Δx, and the time interval, Δt, seems to be at the discretion of the individual. However, some criteria must be met in order to prevent the violation of thermodynamic principles, such as the temperature, $T_i^{t+\Delta t}$, predicted is higher than either $T_{(i-1)}^t$ or $T_{(i+1)}^t$. From Equation 7, such a violation would not occur only when the stability limit is

$$\text{Fo} \leqslant 1/2 \tag{8}$$

Moisture Transfer at the Interior Nodes

For the same interior node 3, according to the law of mass conservation:

Moisture transfer from node 2 + Moisture transfer from node 4 = Rate of change of moisture content for node 3

$$\dot{m}_{2\_3} + \dot{m}_{4\_3} = \rho_b A \Delta x \frac{\partial X}{\partial t}$$

or

$$\rho_b D_{lv} A \frac{X_2^t - X_3^t}{\Delta x} + \rho_b D_{lv} A \frac{X_4^t - X_3^t}{\Delta x} = \rho_b A \Delta x \frac{X_3^{t+\Delta t} - X_3^t}{\Delta t} \tag{9}$$

Solving for $X_3^{t+\Delta t}$

$$X_3^{t+\Delta t} = \text{Fo}_{mass}\,(X_2^t + X_4^t) + (1 - 2\,\text{Fo}_{mass})\, X_3^t \tag{10}$$

In Equation 10,

$$\text{Fo}_{mass} = \frac{D_{lv} \Delta t}{(\Delta x)^2} \tag{11}$$

Obviously, Equation 10 is analogous to Equation 5, in which the temperature of interior node 3 at time $t + \Delta t$ is found.

For an interior node, *i*, Equation 10 can be rewritten as:

$$X_i^{t+\Delta t} = \text{Fo}_{mass}\,(X_{(i-1)} + X_{(i+1)}^t) + (1 - 2\,\text{Fo}_{mass})\, X_i^t \tag{12}$$

Similarly, for Equation 10, the stability limit is:

$$\text{Fo}_{mass} \leqslant 1/2 \tag{13}$$

Such a restriction is more easily satisfied because of the smaller magnitude of the mass diffusivity, D_{lv}.

Heat Transfer at the Surface Nodes

For a one-dimensional heat flow, the energy balance at surface node 1, as shown in Figure 5, gives:

Conductive heat from node 2 + Convective heat transfer from space air + Latent heat of moisture transfer from space air + Radiative heat from electric lighting = Rate of change of internal energy of node 1

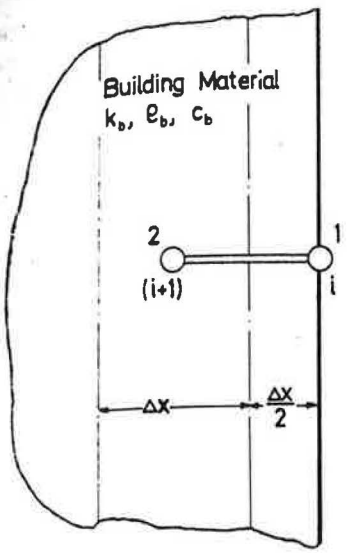

Figure 5 *Surface node in a one-dimensional heat and moisture transfer*

$$kA_1\frac{T_2^t-T_1^t}{\Delta x} + h_{c1}A_1\,(T_r^t-T_1^t) + \rho_a h_{m1}A_1X_1^t\,(w_r^t-w_{1s}^t)\,h_{fg} + L_{r1} = \rho_b c_b A_1\,\frac{\Delta x}{2}\,\frac{T_1^{t+\Delta t}-T_1^t}{\Delta t}$$

Solving for $T_1^{t+\Delta t}$ and rearranging the terms, then

$$T_1^{t+\Delta t} = 2\text{Fo}\left(T_2^t+\text{Bi}\,[T_r^t+\frac{\rho_a h_{m1}h_{fg}X_1^t}{h_{c1}}\,(w_r^t-w_{1s}^t)+\frac{L_{r1}}{h_{c1}A_1}]\right) + [1-2\text{Fo}\,(1+\text{Bi})]\,T_1^t \qquad (14)$$

where Bi is the Biot number and is defined as

$$\text{Bi} = \frac{h_c\Delta x}{k} \qquad (15)$$

For a surface node, *i*, Equation 14 can be rewritten as:

$$T_i^{t+\Delta t} = 2\text{Fo}\left(T_{(i+1)}^t+\text{Bi}\,[T_r^t+\frac{\rho_a h_{mi}h_{fg}X_i^t}{h_{ci}}\,(w_r^t-w_{is}^t)+\frac{L_{ri}}{h_{ci}A_i}]\right) + [1-2\text{Fo}\,(1+\text{Bi})]\,T_i^t \qquad (16)$$

The stability limit of the surface node requires that all the coefficients in Equation 16 be positive, that is:

$$\text{Fo}\,(1+\text{Bi}) \leqslant 1/2 \qquad (17)$$

Moisture Transfer at the Surface Nodes

According to the law of conservation of mass, the following relationship holds for surface node 1:

Moisture transfer from node 2	+	Moisture transfer by convection	=	Rate of change of moisture content for node 1

$$\dot{m}_{2-1} + \dot{m}_{r-1} = \rho_b A\,\frac{\Delta x}{2}\,\frac{\partial X}{\partial t}$$

or

$$\rho_b D_{iv}A\,\frac{X_2^t-X_1^t}{\Delta x} + \rho_a h_m A K_{sc1}X_1^t\,(w_r^t-w_{1s}^t) = \rho_b A\,\frac{\Delta x}{2}\,\frac{X_1^{t+\Delta t}-X_1^t}{\Delta t}$$

Solving for $X_1^{t+\Delta t}$, then

$$X_1^{t+\Delta t} = (1-2\text{Fo}_{mass})X_1^t + 2\text{Fo}_{mass}X_2^t + \frac{2\rho_a}{\rho_b}\,\frac{h_{m1}\Delta t}{\Delta x}\,X_1^t(w_r^t-w_{1s}^t) \qquad (18)$$

For a surface node, *i*, Equation 18 can be rewritten as:

$$X_i^{t+\Delta t} = (1-2\text{Fo}_{mass})X_i^t + 2\text{Fo}_{mass}X_{(i+1)}^t + \frac{2\rho_a}{\rho_b}\,\frac{h_{mi}\Delta t}{\Delta x}\,X_i^t(w_r^t-w_{is}^t) \qquad (19)$$

Heat Transfer at the Window Glass

While the thickness of the window glass is only 5 mm (0.2 in.), for simplicity it is usually assumed that the temperature of the window glass, T_g, is the same in the center of the glass as on the two surfaces. Consider the heat balance at the center of the window glass, node *g*:

Heat transfer from the inside surface of the window glass	+	Heat transfer from the outside surface of the window glass	=	Rate of change of internal energy of the window glass

$$h_{cr}A_g(T_r^t-T_g^t) + h_{co}A_g\,(T_{og}^t - T_g^t) = \rho_g c_g A_g\Delta x_g\,\frac{T_g^{t+\Delta t}-T_g^t}{\Delta t}$$

Solving for $T_g^{t+\Delta t}$

$$T_g^{t+\Delta t} = (1-\frac{h_{cr}\Delta t}{\rho_g c_g\Delta x_g} - \frac{h_{co}\Delta t}{\rho_g c_g\Delta x_g})T_g^t + \frac{\Delta t}{\rho_g c_g\Delta x_g}(h_{cr}T_r^t+h_{co}T_{og}^t) \qquad (20)$$

Surface Temperature of the Plexiglass of the Light Troffer

In comparing the convective and radiative heat transfer from the plexiglass, the heat conduction to the suspended ceiling through the angle iron framework is small and, hence, can be neglected. Then, for a recessed mounted light troffer, the heat released downward into the space air, as shown in Figure 6, consists of mainly: (i) convective heat transfer from the plexiglass, (ii) radiative heat transfer from the plexiglass, and (iii) light energy transmitted through the plexiglass.

Energy balance on the plexiglass of the light troffer during the operating period gives:

Radiative heat transfer from the plexiglass	+	Convective heat transfer from the plexiglass	+	Rate of change of internal energy of the plexiglass	=	Energy of electric lights released downward	−	Energy of visible light downward

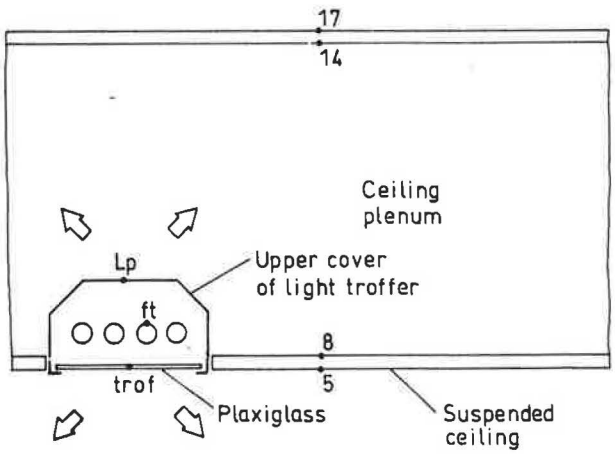

Figure 6 *Thermal model of the light troffer*

$$h_{r\cdot trof} A_{trof} (T^t_{trof} - T^t_{1\text{-}9}) + h_{c\cdot trof} A_{trof} (T^t_{trof} - T^t_r) + m_{trof} c_{trof} \frac{T^{t+\Delta t}_{trof} - T^t_{trof}}{\Delta t} = (K_d - K_{vl}) L_w \quad (21)$$

$T_{1\text{-}9}$ indicates the average surface temperature of the partition wall and floor at time t, °C. For the sake of simplicity

$$T^t_{1\text{-}9} \cong \frac{1}{2}(T_1 + T_9) \quad (22)$$

Solving for T_{trof},

$$T^{t+\Delta t}_{trof} = \left(1 - \frac{h_{c\cdot trof} A_{trof} \Delta t}{m_{trof} c_{trof}} - \frac{h_{r\cdot trof} A_{trof} \Delta t}{m_{trof} c_{trof}}\right) T^t_{trof} + \frac{h_{c\cdot trof} A_{trof} \Delta t}{m_{trof} c_{trof}} T^t_r + \frac{h_{r\cdot trof} A_{trof} \Delta t}{m_{trof} c_{trof}} T^t_{1\text{-}9} + \frac{\Delta t}{m_{trof} c_{trof}} (K_d - K_{vl}) L_w \quad (23)$$

During the off-period, the term L_w in Equation 23 is equal to zero. This causes the decrease of T_{trof}.

Surface Temperature of the Upper Cover of the Light Troffer

Energy balance at the upper cover of the light troffer during the operating period shows:

Radiative heat transfer from the upper cover	+	Convective heat transfer from the upper cover	+	Rate of change of internal energy of upper cover	=	Energy of electric lights released upward

$$h_{r\cdot lp} A_{lp} (T^t_{lp} - T^t_{14}) + h_{c\cdot lp} A_{lp} (T^t_{lp} - T^t_p) + m_{lp} c_{lp} \frac{T^{t+\Delta t}_{lp} - T^t_{lp}}{\Delta t} = K_{up} L_w$$

Solving for $T^{t+\Delta t}_{lp}$,

$$T^{t+\Delta t}_{lp} = \left(1 - \frac{h_{r\cdot lp} A_{lp} \Delta t}{m_{trof} c_{trof}} - \frac{h_{r\cdot trof} A_{trof} \Delta t}{m_{trof} c_{trof}}\right) T^t_{trof} + \frac{h_{c\cdot trof} A_{trof} \Delta t}{m_{trof} c_{trof}} T^t_r + \frac{h_{r\cdot trof} A_{trof} \Delta t}{m_{trof} c_{trof}} T^t_{1\text{-}9} + \frac{\Delta t}{m_{trof} c_{trof}} (K_d - K_{vl}) L_w \quad (24)$$

The fraction of energy of electric lights released upward or downward can be determined from the tests in the test chamber.

Space and Plenum Air Temperature

In the calculation of the air temperature inside the test chamber or in the ceiling plenum, the following differences between the operating period and the off-period must be taken into account:

1. Cold air is supplied to the test chamber during the operating period. A portion of the supply air is infiltrated into the ceiling plenum through the gaps of the suspended ceiling. On the other hand, there is no conditioned air supplied to the test chamber during the off-period and none of the conditioned air is infiltrated into the ceiling plenum during the off-period.
2. Electric lighting and the warm air heater are switched on during the operating period. Therefore, the heat released from the light troffer and the heater are the major heat sources in the test chamber and the ceiling plenum during the operating period. During the off-period, the electric lights and the heater are switched off. The heat released from the data acquisition unit and the heat storage of the light troffer are the major heat sources in that period.
3. Because of the small rate of change of internal energy of the space air or the plenum air itself compared with the heat released from the light troffer and the heater during the operating period, it is assumed that the space air and the plenum air both have no thermal capacity during the operating period. Nevertheless, the rate of change of the internal energy of the space air and the plenum air should be taken into account during the off-period.
4. Due to the fact that the conditioned air supplied to the test chamber or the infiltrated conditioned air in the ceiling plenum forms a forced convection upon various surfaces of the building envelope, considerably higher convective heat transfer coefficients and mass transfer coefficients will be used for heat and moisture transfer during the operating period. While in the off-period, air flow is mainly due to the density difference of the airstreams, which results from a free convection on various surfaces of the test chamber. Lower convective heat and mass transfer coefficients will be used.

Space and Plenum Air Temperature During the Operating Period

Heat balance on the space air or the plenum air gives the following relationship:

Internal energy of supply air	+	Convective heat transfer from building envelope	+	Convective heat transfer from internal loads	+	Heat gain due to infiltrated air	=	Internal energy of space air

$$\dot{V}_s \rho_s c_{pa} T^{t+\Delta t}_s + \sum_{i=1}^{n} h_{ci} A_i (T^{t+\Delta t}_i - T^{t+\Delta t}_r) + L_c + O_c + E_e + \dot{V}_{if} \rho_{if} c_{pa} (T^{t+\Delta t}_{if} - T^{t+\Delta t}_r) = \dot{V}_s \rho_s c_{pa} T^{t+\Delta t}_r \quad (25)$$

During the operating period there is no occupant in the test chamber and only exfiltrated air discharges from the test chamber. Also, the radiative fraction of heat transfer from the warm air heater and the data acquisition unit is small. For the sake of simplicity, all the electric power input to the heater and data acquisition unit is considered as the convective heat transfer. Then, the heat balance on the space air can be expressed as:

$$\dot{V}_s \rho_s c_{pa} T^{t+\Delta t}_s + \sum_{i=1}^{n} h_{ci} A_i (T^{t+\Delta t}_i - T^{t+\Delta t}_r) + h_{c\cdot trof} A_{trof} (T^{t+\Delta t}_{trof} - T^{t+\Delta t}_r) + E_h + E_{da} = \dot{V}_s \rho_s c_{pa} T^{t+\Delta t}_r$$

Solving for $T^{t+\Delta t}_r$,

$$T^{t+\Delta t}_r = \frac{\dot{V}_s \rho_s c_{pa} T^{t+\Delta t}_s + \sum_{i=1}^{n} h_{ci} A_i T^{t+\Delta t}_i + h_{c\cdot trof} A_{trof} T^{t+\Delta t}_{trof} + E_h + E_{da}}{\dot{V}_s \rho_s c_{pa} + \sum_{i=1}^{n} h_{ci} A_i + h_{c\cdot trof} A_{trof}} \quad (26)$$

In the ceiling plenum, only a fraction, K_{leak}, of conditioned air is leaked into the plenum and, hence, heat balance on the plenum air gives:

$$K_{leak}\dot{V}_s\rho_s c_{pa}T_s^{t+\Delta t} + \sum_{j=1}^{n} h_{cj}A_j\,(T_j^{t+\Delta t} - T_p^{t+\Delta t}) + h_{c\cdot lp}A_{lp}\,(T_{lp}^{t+\Delta t} - T_p^{t+\Delta t}) = K_{leak}\dot{V}_s\rho_s c_{pa}T_p^{t+\Delta t}$$

Subscript j represents the number of surfaces of the convective heat transfer in the ceiling plenum. Solving for $T_p^{t+\Delta t}$, then

$$T_p^{t+\Delta t} = \frac{K_{leak}\dot{V}_s\rho_s c_{pa}T_s^{t+\Delta t} + \sum_{j=1}^{n} h_{cj}A_j\,T_j^{t+\Delta t} + h_{c\cdot lp}A_{lp}T_{lp}^{t+\Delta t}}{K_{leak}\dot{V}_s\rho_s c_{pa} + \sum_{j=1}^{n} h_{cj}A_j + h_{c\cdot lp}A_{lp}} \qquad (27)$$

Space and Plenum Air Temperature During the Off-Period

The results of the principal tests showed that the surface temperature of the building envelope was about 0.2°C to 0.3°C lower than the adjacent air during the off-period. Therefore, the heat released from the data acquisition unit and the heat transfer from the plexiglass to the space air were convected to the building envelope during the off-period. Heat balance on the space air at the off-period gives:

Convective heat transfer from the plexiglass	+	Heat released from the data acquisition unit	=	Convective heat transfer to the building envelope	+	Rate of change of internal energy of the space

$$h_{c\cdot trof}A_{trof}\,(T_{trof}^{t+\Delta t} - T_r^{t+\Delta t}) + E_{da} = \sum_{i=1}^{n} h_{ci}A_i\,(T_r^{t+\Delta t} - T_i^{t+\Delta t}) + \frac{\dot{V}_c\rho_a c_{pa}\,(T_r^{t+\Delta t} - T_r^t)}{\Delta t} \qquad (28)$$

Instead of using the forward difference method in Equation 28, a backward difference method is adopted. This is because of the possibility of having unstable $T_r^{t+\Delta t}$ if a forward difference method is applied. Moreover, in Equation 28, $T_i^{t+\Delta t}$ and $t_{trof}^{t+\Delta t}$ are all known values, therefore, the disadvantage of solving a number of algebraic equations does not exist in such a circumstance. Since the differences between $T_r^{t+\Delta t}$ and T_r^t, and between $T_i^{t+\Delta t}$ and T_i^t and $T_{trof}^{t+\Delta t}$ and T_{trof}^t are so small, such an alternation is considered suitable.

Let $\mathbf{Z} = \Delta t/(\dot{V}_c\Delta_a c_{pa})$; then solving for $T_r^{t+\Delta t}$,

$$T_r^{t+\Delta t} = \frac{\mathbf{Z}E_{da} + \mathbf{Z}h_{c\cdot trof}A_{trof}\,T_{trof}^{t+\Delta t} + \mathbf{Z}\sum_{i=1}^{n} h_{ci}A_i\,T_i^{t+\Delta t} + T_r^t}{\mathbf{Z}h_{c\cdot trof}A_{trof} + \mathbf{Z}\sum_{i=1}^{n} h_{ci}A_i + 1} \qquad (29)$$

Heat balance on the plenum air during the off-period can be expressed as:

Convective heat transfer from the upper cover of the light troffer	=	Convective heat transfer between the plenum air and other surface	+	Rate of change of internal energy of plenum air

$$h_{c\cdot lp}A_{lp}\,(T_{lp}^{t+\Delta t} - T_p^{t+\Delta t}) \sum_{i=1}^{n} h_{ci}A_i\,(T_p^{t+\Delta t} - T_i^{t+\Delta t}) + \dot{V}_p\rho_a c_{pa}\frac{T_p^{t+\Delta t} - T_p^t}{\Delta t} \qquad (30)$$

Let $\mathbf{Y} = \Delta t/\dot{V}_p\rho_a c_{pa}$; then solving for $T_{lp}^{t+\Delta t}$,

$$T_{lp}^{t+\Delta t} = \frac{\mathbf{Y}h_{c\cdot lp}A_{lp}\,T_{lp}^{t+\Delta t} + \mathbf{Y}\sum_{i=1}^{n} h_{ci}A_i\,T_i^{t+\Delta t} + T_p^t}{\mathbf{Y}h_{c\cdot lp}A_{lp} + \mathbf{Y}\sum_{i=1}^{n} h_{ci}A_i + 1} \qquad (31)$$

Space Humidity Ratio

In the test chamber, a moisture transfer from the building envelope to the space air exists during the operating period because of the significant drop in the space humidity ratio after the supply of conditioning air. While in the off-period, because of the possible water vapor diffusion from the wetted surfaces in the water spraying chamber and also the infiltration of more humid air from the buffer zone, the space humidity ratio is often higher than during the operating period. A moisture transfer from the space air to the building envelope exists during the off-period.

The rate of moisture transfer from the building envelope to the space air during the operating period at time $t+\Delta t$, $\dot{m}_w^{t+\Delta t}$ is:

$$\dot{m}_w^{t+\Delta t} = \sum_{i=1}^{n} \rho_a h_{mi}X_i^{t+\Delta t}\,(w_{is}^{t+\Delta t} - w_r^{t+\Delta t}) \qquad (32)$$

This is the only latent load in the test chamber during the operating period. Then, the space humidity ratio can be calculated as:

$$w_r^{t+\Delta t} = w_s^{t+\Delta t} + \frac{\dot{m}_w^{t+\Delta t}}{\dot{V}_s\rho_s} = w_s^{t+\Delta t} + \frac{1}{\dot{V}_s\Delta_s}\sum_{i=1}^{n} \rho_a h_{mi}A_i\,X_i^{t+\Delta t}\,(w_{is}^{t+\Delta t} - w_r^{t+\Delta t}) \qquad (33)$$

Substituting Equation 32 into Equation 33 and solving for $w_r^{t+\Delta t}$,

$$w_r^{t+\Delta t} = \frac{1}{\frac{1}{\dot{V}_s\rho_s}\sum_{i=1}^{n} \rho_a h_{mi}A_i\,X_i^{t+\Delta t}\,w_{is}^{t+\Delta t} + \frac{1}{\dot{V}_s\rho_s}\sum_{i=1}^{n} \rho_a h_{mi}A_i\,X_i^{t+\Delta t}\,w_{is}^{t+\Delta t}}\,w_s^{t+\Delta t} \qquad (34)$$

The space latent load, q_{rl}, can be calculated as:

$$q_{rl} = \dot{m}_w h_{fg} \qquad (35)$$

The degree of saturation of the space, which is approximately equal to the space relative humidity, is:

$$\phi_r^{t+\Delta t} \cong \mu^{t+\Delta t} = \frac{W_r^{t+\Delta t}}{W_{sr}^{t+\Delta t}} \tag{36}$$

In Equation 36, $w_{sr}^{t+\Delta t}$ indicates the humidity ratio of saturated air at space temperature, and

$$w_{sr}^{t+\Delta t} = a_1 + b_1 T_r^{t+\Delta t} + c_1 (T_r^{t+\Delta t})^2 + d_1 (T_r^{t+\Delta t})^3 \tag{37}$$

where

$a_1 = 3.768 \times 10^{-3}$
$b_1 = 3.0517 \times 10^{-4}$
$c_1 = 4.648 \times 10^{-6}$
$d_1 = 3.787 \times 10^{-7}$

During the off-period, the water vapor diffusion and the infiltrated air from the external sources are difficult to evaluate, therefore, the space humidity ratio cannot be determined according only to the moisture transfer between the space air and the building envelope.

Space Sensible Cooling Load

After the surface temperature of various surfaces of the building envelope in the test chamber has been determined, then the space sensible cooling load during the operating period, $q_{rs}^{t+\Delta t}$, in the test chamber can be evaluated as:

$$q_{rs}^{t+\Delta t} = \sum_{i=1}^{n} h_{ci} A_i (T_i^{t+\Delta t} - T_r^{t+\Delta t}) + h_{c\cdot trof} A_{trof} (T_{trof}^{t+\Delta t} - T_r^{t+\Delta t}) + E_h + E_{da} \tag{38}$$

Properties of Building Materials and the Dimensionless Groups

Calculation of the temperature and moisture content of the surface and interior nodes during the simulation of the space operating characteristics of the test chamber, and the properties of the building materials are listed in Table 5. Hence, the dimensionless groups:

$$\text{Fo} = \frac{\alpha \Delta t}{(\Delta x)^2}$$

$$\text{Fo}_{mass} = \frac{D_{iv} \Delta t}{(\Delta x)^2}$$

$$\text{Bi} = \frac{h_c \Delta x}{k}$$

for various nodes can thus be calculated.

TABLE 5
Properties of the Building Materials

Material	Density kg/m³ (lb/ft³)	Thermal conductivity k, W/m·K (Btu/h·ft·°F)	Specific heat, c J/kg·K (Btu/lb·°F)	Mass diffusivity D_{iv} m²/s (ft²/s)
Acoustic tile	359 (22.4)	0.07 (0.0404)	800 (0.191)	1×10^{-8} (1.08×10^{-7})
Wood (hard)	650 (40.6)	0.165 (0.0953)	1630 (0.389)	1×10^{-9} (1.08×10^{-8})
Glass	2500 (156)	1.05 (0.607)	840 (0.200)	

Simulated Space Sensible Cooling Load Compared Against Measured Readings

The only way to assess the accuracy of the simulation of simultaneous heat and moisture transfer in the test chamber is to compare the simulated values against the actual measured readings. The following is the comparison between the simulated values and the actual measured readings on July 28, 1988. On that date, the test chamber had been operated in the nighttime shutoff mode at a fan motor speed of 650 rpm for more than two day-and-night cycles.

The simulating space sensible load, q_{rs}, in the test chamber was calculated by Equation 38. The actual space sensible heat extraction rate, $q_{ex\cdot s}$, calculated from the measured $T_r^{t+\Delta t}$ and $T_s^{t+\Delta t}$ readings, is equal to $q_{rs}^{t+\Delta t}$ as the $T_r^{t+\Delta t}$ is the same at time $t+\Delta t$. The sensible heat extraction rate can be calculated as:

$$q_{ex\cdot s}^{t+\Delta t} = q_{rs}^{t+\Delta t} = \dot{V}_s \rho_s c_{pa} (T_r^{t+\Delta t} - T_s^{t+\Delta t}) \tag{39}$$

In Figure 7, the upper light dots indicate the points plotted from the simulated values, $q_{rs}^{t+\Delta t}$, and the heavy dots represent the actual measured $q_{ex\cdot s}^{t+\Delta t}$ readings.

First, the simulated values, q_{rs}, were deviated from the actual measured readings at a range of only 60 to 5 W (205 to 17 Btu/h) before noon. In the afternoon, the deviations were significantly reduced.

Second, the simulated values showed a trend of inclining downward slightly in the cool-down period. After that, q_{rs} fluctuated between 635 W (2167 Btu/h) and 593 W (2024 Btu/h) until 16:52 p.m., whereas the actual measured $q_{ex\cdot s}$ also showed a slightly downward trend in the same period, then fluctuated between 601 W (12,051 Btu/h) and 552 W (1884 Btu/h) before noon and showed a slightly upward trend to a maximum of 617 W (2106 Btu/h) just before the air handler was turned off at 16:54 p.m.

Electric lighting and the warm air heater are the dominating internal loads in this test chamber. The slightly downward trend of the q_{rs} is mainly due to the sudden drop of space temperature $T_r^{t+\Delta t}$. Such a drop is then compensated by the increase of the convective heat transfer from the plexiglass of the light troffer.

The increase of $q_{ex\cdot s}$ after 13:00 p.m. is mainly because of the increased temperature difference $(T_r^{t+\Delta t} - T_s^{t+\Delta t})$.

Simulated Space Latent Cooling Load Compared Against Measured Readings

The simulated latent loads were calculated using Equations 32 and 35. The actual space latent heat extraction rate is given by:

$$q_{ex\cdot l} = \dot{V}_s \rho_s (w_r^{t+\Delta t} - w_s^{t+\Delta t}) h_{fg} \tag{40}$$

In Figure 7, the simulated $q_{rl}^{t+\Delta t}$ values are indicated by the light dots in the lower part of the figure, and the actual measured $q_{ex\cdot l}$ are shown by the crosses.

It is interesting to see that the simulated q_{rl} values agree with the $q_{ex\cdot l}$ values calculated from the measured $w_r^{t+\Delta t}$, $w_s^{t+\Delta t}$, and the supply volume flow rates, $\dot{V}_s$. Their mean value difference is about 20 W (68 Btu/h) before noon. In the afternoon, the deviation increases to 40 W (137 Btu/h). Both simulated $q_{rl}^{t+\Delta t}$ values and actual $q_{ex\cdot s}^{t+\Delta t}$

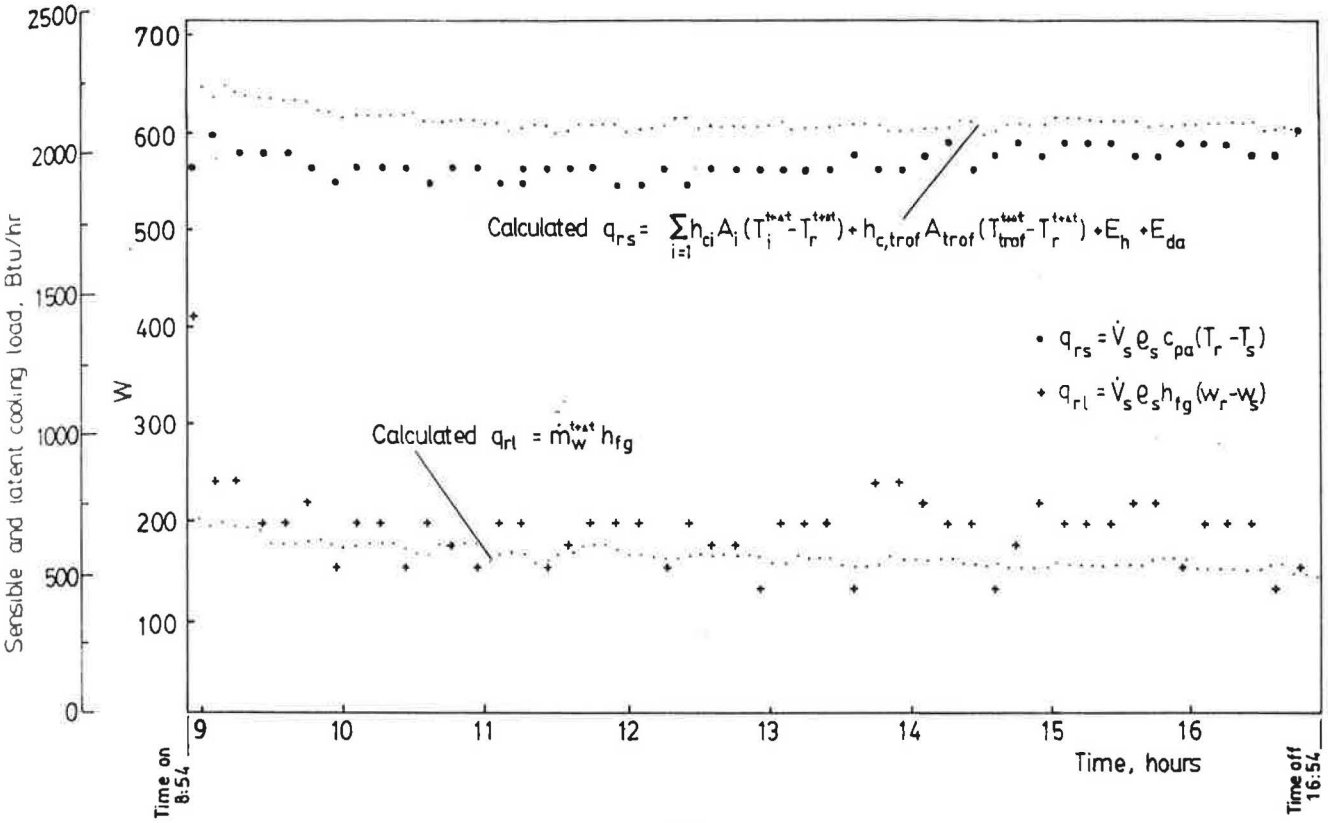

Figure 7 *Calculated q_{rs} and q_{rl} values based on measured $T_r - T_s$ and $w_r - w_s$ compared against q_{rs} and q_{rl} values from system simulation*

values showed a slightly downward trend before 10:00 a.m. After that, the downward trend is not as significant.

Because of the lack of occupants in the test chamber during the operating period, the space latent load, $q_{rl}^{t+\Delta t}$, or the latent heat extraction rate, $q_{ex,l}$, is mainly due to the moisture transfer from the building structures.

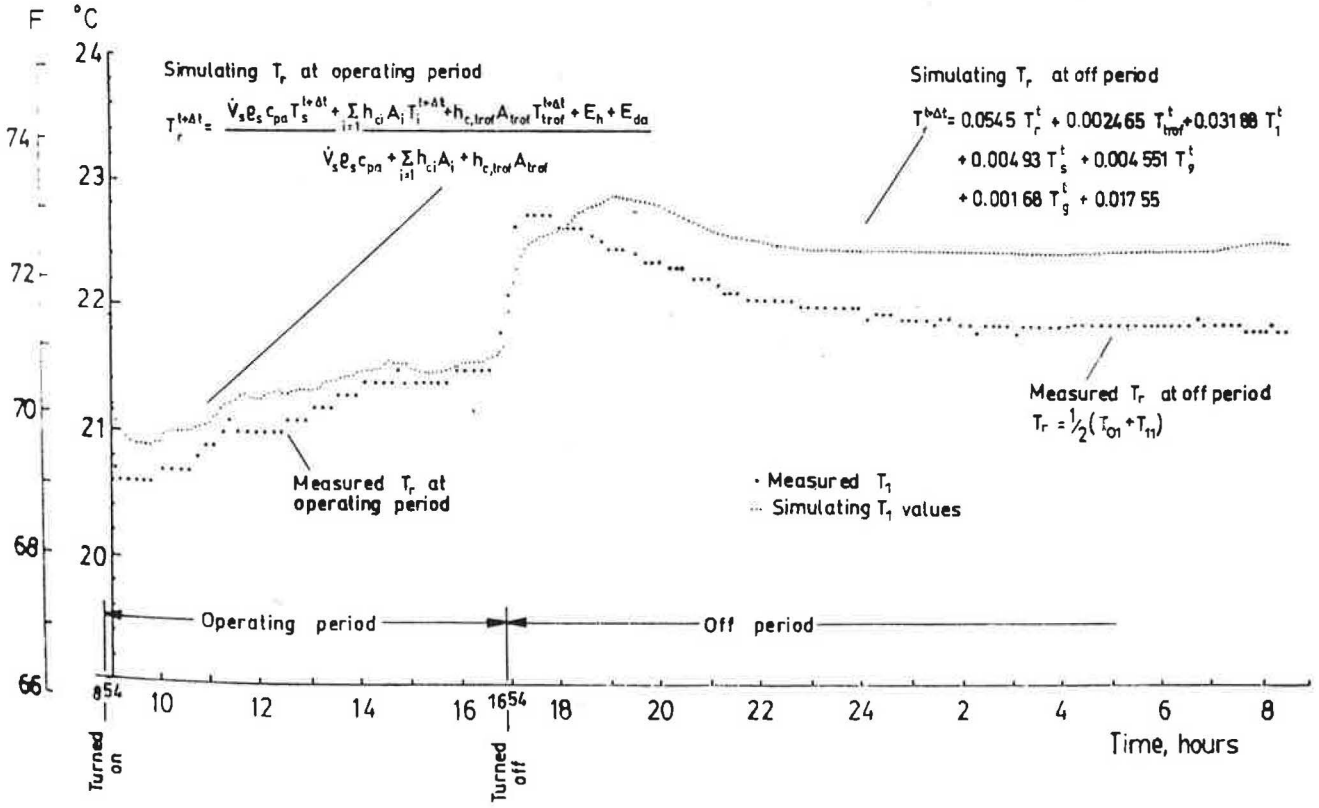

Figure 8 *Measured space temperature, T_r, compared against simulated values*

Simulated Space Air Temperature Compared Against Measured Readings

The simulated space air temperature, $T_r^{t+\Delta t}$, of the test chamber during the operating period was calculated by Equation 26 and during the off-period was given by Equation 29. In Figure 8, the fine dots show the simulated $T_r^{t+\Delta t}$ values during the operating period between 8:54 a.m. and 16:54 p.m., and also during the off-period between 16:54 p.m. and 8:20 a.m. The heavy circular dots represent the measured $T^{t+\Delta t}$ readings during both the operating and the off-periods.

In Figure 8, the simulated $T_r^{t+\Delta t}$ agrees with the measured values during the operating period. The simulated $T_r^{t+\Delta t}$ deviates only about 0.3°C (0.54°F) to 0.1°C (0.18°F) from the actual measured readings. During the off-period, the simulated $T_r^{t+\Delta t}$ was about 0.6°C higher than the actual measured readings after 22:00 p.m. This is mainly due to:

(i) During the operating period, there is a more accurate space sensible cooling load, $q_{rs}^{t+\Delta t}$, a more stable supply air volume flow rate, $\dot{V}_s$, and a precisely measured supply air temperature, $T_s^{t+\Delta t}$, and return temperature, $T_r^{t+\Delta t}$. There also is no infiltration air during the operating period. Although the space sensible cooling load, $q_{rs}^{t+\Delta t}$, is so small during the off-period, its magnitude is difficult to determine precisely. Also, it is more difficult to determine the amount of infiltrated air entering the chamber or the exfiltrated air leaving the chamber during the off-period.

(ii) The mean convective heat transfer coefficient, h_c, along the surface of the building structure at force convection can be found from more reliable sources. The current dimensionless correlation to determine h_c values for the building envelope at free convection may be quite different from actual values.

(iii) It is difficult to find mean values of air temperature and air velocities in the test chamber at free convection during the off-period.

In Figure 8, the simulated $T_r^{t+\Delta t}$ values had a smaller sudden drop just after the air handler was turned on and also a slower rise in $T_r^{t+\Delta t}$ values just after the air handler was turned off. These deviations showed that the simulated $T_r^{t+\Delta t}$ had a greater heat storage effect.

Simulated and Measured Space Humidity Ratio and Relative Humidity During the Operating Period

The simulated humidity ratios were calculated by Equation 34 and the actual measured space humidity ratios were determined from the measured dry- and wet-bulb of the return airstream by using the psychrometric chart.

In Figure 9, the upper figure shows the simulated and actual measured space humidity ratios. The crosses indicate the actual measured space humidity ratios and the light dots represent the simulated space humidity ratios.

Apparently, the difference between the simulated and measured values is rather small. Most of the points have a difference of about 0.0001 kg/kg (0.0001 lb/lb) to 0.0002 kg/kg (0.0002 lb/lb), which is less than 2%. Again, both the simulated and actual measured values have a tendency to increase with time.

The simulated relative humidities were calculated from Equations 34, 36, and 37. The actual measured relative humidities were determined from the measured dry- and wet-bulb of the return airstream by using the psychrometric chart.

In Figure 9, the lower figure shows the simulated and actual measured space relative humidities. The light dots

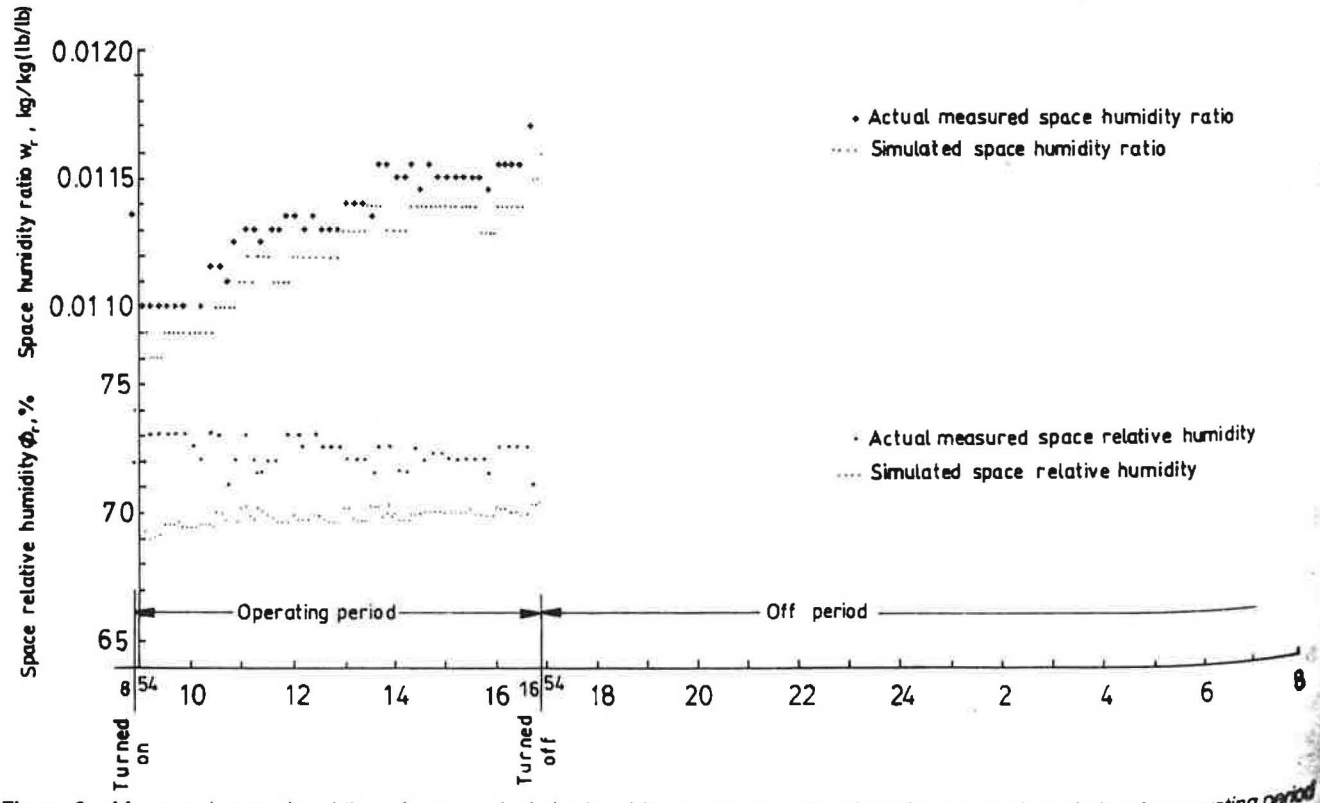

Figure 9 *Measured space humidity ratio, w_r, and relative humidity, ϕ_r, compared against simulated values during the operating period*

indicate the simulated space relative humidities, and the heavy dots the actual measured ones.

From the heavy and light dots in Figure 9, it is obvious that the difference between the simulated and actual measured space relative humidities is small, and the actual measured space relative humidity is about 3% higher than the simulated values.

Both the actual measured space relative humidities and the simulated values remain quite stable during the operating period.

Simulated and Measured Space Humidity Ratio and Space Relative Humidity During the Off-Period

During the off-period, it is difficult to find out the mean space humidity ratio, w_r, and the mean space relative humidity, ϕ_r.

It is also difficult to find out the simulated mean w_r and ϕ_r because of the undetermined amount of infiltrated moisture into the space from various external sources.

Again, it is difficult to determine the actual measured mean space relative humidity from the measured dry- and wet-bulb from dry and wetted thermocouples under free convection.

From the continuous record of a thermohygrograph whose location is in the vicinity of the center of the south partition wall (see Figure 1), the air relative humidity was gradually increased at an amount of about 2% during the off-period from July 28, 1988 (16:54 p.m.) to July 29, 1988 (8:58 a.m.).

Simulated Surface Temperature of Partition Wall Compared Against Measured Readings

Figure 10 shows the measured and simulated surface temperatures of the partition wall, T_1, and the measured air temperature adjacent to the surface temperature of the partition wall.

In Figure 10, the following trends are obvious:

(i) Both the measured and simulated T_1 dropped suddenly in the cool-down period. The sudden drop of T_1 was mainly because of the drop in the space air temperature, T_r, and the need of latent heat of vaporization. Their values rose gradually during the operating period due to the increase in space temperature, T_r, and the heat absorbed from electric lights.

(ii) During the operating period, the simulated T_1 were about 0.3°C (0.54°F) lower than the actual measured values. Since the surface temperature, T_1, at time $t+\Delta t$ during most of the operating period was lower than the T_1 value just before the air system was turned on, a space sensible cooling load existed due to the heat transfer from the building structures to the space air.

(iii) Both the measured and simulated T_1 rose sharply after the air system was turned off. The simulated T_1 showed a greater heat storage effect. After that, T_1 inclined downward gradually during the off-period. The simulated T_1 values agree with the measured values during the off-period.

(iv) The measured air temperature adjacent to surface T_1 was about 0.2°C (0.36°F) lower than T_1 during the operating period. It was about 0.2°C (0.36°F) higher than the surface temperature T_1 during the off-period.

Parameters Influence the Test Chamber Characteristics During Operating Period

In the simulation of simultaneous heat and moisture

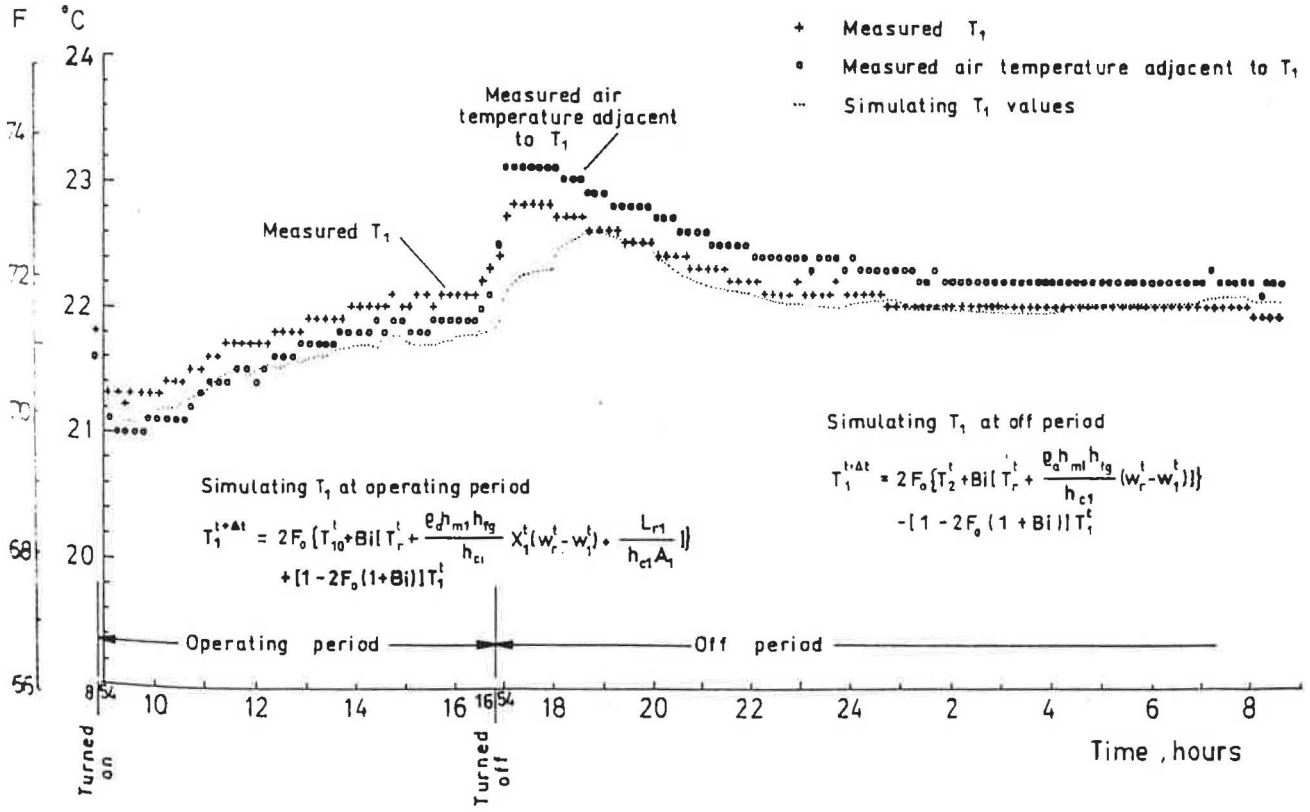

Figure 10 Measured surface temperature of partition wall, T_1, compared against simulated values

transfer between the building envelope and the space air during the operating period in the test chamber, the space cooling load due to a warm air electric heater and a data logger is a constant, that is, 300 + 16 = 316 W (1079 Btu/h). The parameters that influence the simulated values of the space sensible cooling load, $q_{rs}^{t+\Delta}$, space latent cooling load, $q_{rl}^{t+\Delta}$, space air temperature, $T_r^{t+\Delta}$, surface temperature of partition wall, $T_1^{t+\Delta}$, and surface temperature of the floor, $T_9^{t+\Delta}$, are mainly due to:

(i) mean convective heat transfer coefficient, h_c;
(ii) mean convective mass transfer coefficient, h_m, indicated in terms of $K_m h_m$;
(iii) effective contact area, XA_s, indicated in terms of $K_A XA_s$; and
(iv) downward portion of the visible light transmitted through the plexiglass of the light troffer.

As the convective mass transfer coefficient, h_m, is linked to the convective heat transfer coefficient, h_c, according to the Chilton-Colburn analogy, both the variations of $K_A XA_s$ and h_c values in Equation 32 influence the moisture transfer.

Although mass diffusivity, D_{lv}, influences the moisture content of the building structure, $X_l^{t+\Delta}$, and hence, the heat and moisture transfer in the test chamber during the hot and humid summer days in the tropical zone, the moisture content of the portion of the building structure adjacent to the space air tends to revert to its original higher value just before the starting of the air handler because of the higher space relative humidity, ϕ, and space humidity ratio, w_r, during the off-period.

Table 6 lists the results of simultaneous heat and moisture transfer simulations when one of the parameters changes and, at the same time, most of the others remain unchanged.

In Table 6, five system simulations have been completed to compare the simulated values of q_{rs}, q_{rl}, T_r^t, T_1^t, and T_9^t.

In the test chamber, the total wattage of the electric lights is calculated as: 16 × 65 × 1.1 = 1145 W (3908 Btu/h). During the simulation, the downward portion of the visible light had been assumed to be 0.15 and 0.2 of the total lighting wattage. Hence, the total downward portion had been changed from 0.35 to 0.4.

The values of q_{rs}, q_{rl}, T_r^t, T_1^t, and T_9^t in Table 6 are the simulated mean of the three consecutive values at 11:56 a.m., 12:01 p.m., and 12:06 p.m. during the operating period. The reason a mean value is used around noon is because it is more representative in comparison.

Increase of the Value of the Convective Mass Transfer Coefficient, $K_m h_m$, and Effective Contact Area, $K_A XA_S$

In Table 6, when the factor K_m or K_A increases from 0.5 to 1.5, there is:

(i) a corresponding increase of space latent cooling load, q_{rl}, from 93 W to 225 W (317 Btu/h to 768 Btu/h) and a drop of space sensible cooling, q_{rs}, from 636 W to 582 W (2171 Btu/h to 1986 Btu/h);
(ii) an increase of total space cooling load, $q_{rc} = q_{rs} + q_{rl}$, from 729 W to 807 W (2488 Btu/h to 2754 Btu/h);
(iii) a considerable drop in the surface temperature of partition wall T_1 from 21.74°C to 21.33°C (71.1°F to 70.4°F) and in the surface temperature of the floor from 21.74°C to 21.29°C (71.1°F to 70.3°F);
(iv) a decrease in space air temperature, T_r, from 21.47°C to 21.14°C (70.6°F to 70.1°F); and
(v) a drop in temperature difference, T_{1-r}, from 0.27°C to 0.19°C (0.49°F to 0.34°F); and hence, a drop in space sensible cooling load, q_{rs}.

The increase of total space cooling load, T_r, is mainly due to the increase of moisture transfer from the building structures. The increase of q_{rl} results in a decrease of T_r and T_9 and also T_{1-r} and, therefore, the space sensible cooling load, q_{rs}.

Increase in the Value of the Convective Heat Transfer Coefficient, h_c

When the value of the convective heat transfer coefficient has been increased from the empirical formula: $h_c = 5.6 + 3.9v$ to $h_c = 7 + 10v$ because of the Chilton-Colburn analogy, there is a corresponding increase in the convective mass transfer coefficient, h_m; hence there is:

(i) a corresponding increase in the space latent cooling load, q_{rl};
(ii) an increase in the total space cooling load, q_{rc};
(iii) a corresponding drop in the surface temperature of the building structure;
(iv) a slight drop in the space temperature because of the drop in the surface temperature of the building structure;
(v) a significant drop in temperature difference between

TABLE 6
Factors Influencing the Parameters in the Test Chamber During System Simulation

No. of Simulation	h_c	K_m or K_A	Electric Lights: Percentage downward	Electric Lights: Percentage of visible light downward	Space Cooling Load, W(Btu/h): Sensible q_{rs}	Latent q_{rl}	Total q_{rc}	T_r °C (°F)	T_1 °C (°F)	T_9 °C (°F)	$\Delta T_{1-r} = T_1 - T_r$ °C (°F)
1	7+10v	1	0.45	0.175	625 (2133)	179 (611)	840 (2744)	21.41 (70.5)	21.66 (71.0)	21.66 (71.0)	0.25 (0.45)
2	7+10v	1.5	0.4	0.15	582 (1986)	225 (768)	807 (2754)	21.14 (70.1)	21.33 (70.4)	21.29 (70.3)	0.19 (0.34)
3	7+10v	1	0.4	0.15	606 (2068)	166 (567)	772 (2635)	21.29 (70.3)	21.51 (71.3)	21.50 (70.7)	0.22 (0.40)
4	7+10v	0.5	0.4	0.15	636 (2171)	93 (317)	729 (2488)	21.47 (70.6)	21.74 (71.1)	21.74 (71.1)	0.27 (0.49)
5	7+10v	1	0.35	0.15	586 (2000)	153 (625)	739 (2522)	21.17 (70.1)	21.36 (70.4)	21.33 (70.4)	0.19 (0.34)

the surface temperature of the building structure and the space air temperature; and

(vi) although the increase in the h_c enhances the convective heat transfer from the building structure, such an enhancement has been compensated mostly by the drop of the temperature difference between the surface temperature of the building structure and the space air temperature. On the other hand, the increase of q_{rl} causes a considerable drop of q_{rs} and, hence, the final result is a drop of space sensible cooling load, q_{rs}.

Increase in the Energy of Electric Light Downward

When the percentage of the energy of electric light rradiated downward from the light troffer has been increased from 0.35 to 0.45, there is:

(i) a corresponding increase of space sensible cooling load, q_{rs}, from 586 W to 625 W (2000 Btu/h to 2133 Btu/h) and an increase in total space cooling load from 739 W to 804 W (2522 Btu/h to 2744 Btu/h). Both of these increases are smaller than $0.1 \times 1145 = 114.5$ W (391 Btu/h). This is because a portion of the radiative heat is stored inside the building structure. It would not appear as a space cooling load instantaneously.

(ii) a corresponding increase in surface temperature, T_1, from 21.36°C to 21.66°C (70.4°F to 71.0°F), an increase in the surface temperature, T_9, from 21.33°C to 21.66°C (70.4°F to 71.0°F), and an increase in the space temperature, T_r, from 21.17°C to 21.41°C (70.1°F to 70.5°F).

Apparently, an increase of radiative heat on various surfaces of the building structure raises their surface temperature, the space sensible load, q_{rs}, and hence, the space temperature, T_r.

(iii) an increase in the temperature difference between the partition wall and space air, T_{1-r}, and between the floor surface temperature and space air, T_{9-r}. The increase in q_{rs} is accomplished through the enhancement of the temperature difference between the surfaces of building structures and the space air.

FUTURE RESEARCH

This paper only shows some of the research work of the simultaneous heat and moisture transfer between the building envelope and conditioned air when an air system is operated in the nighttime shutdown mode in a tropical area.

In the future, more research needs to be completed to determine the convective mass transfer coefficients for both forced convection and free convection, mass diffusivities, the humidity ratio at the surface of the building material, and the moisture migration at the interface of two layers of different material.

More research will be required to evaluate the moisture migration to the space air through various paths during the off-period. This is the necessary step prior to providing the system simulation of the simultaneous heat and moisture transfer during the off-period.

Of course, there is also a need to have more research to link the simultaneous heat and moisture transfer between the building envelope and space air during the operating period and the off-period with space cooling load calculation in practical, simplified, tabular form.

CONCLUSIONS

1. When the air system is operated under nighttime shutdown conditions, both the actual measured and simulated space sensible cooling load curves of the test chamber inclined downward slightly in the cool-down period. After that, the mean space sensible cooling load remained approximately the same. Only the actual measured space sensible cooling load showed a slight increase in the afternoon. The difference between the simulated and actual measured space sensible cooling load is acceptable.
2. The simulated and actual measured space latent loads both showed a slightly downward trend during the cool-down period. The space latent load in the test chamber was mainly formed because of the moisture transfer from the building structures during the operating period. The simulated space latent load deviated moderately from the actual measured values.
3. Both the simulated and actual measured space air temperatures had a sudden drop after the air handler was turned on. The space air temperature was then increased gradually due to the rise of the supply air temperature. The simulated space air temperature agreed with the actual measured values during the operating period. The discrepancy increased to a considerable value during the off-period because of many uncertainties.
4. The actual measured space humidity ratio showed an upward trend due to the increase of the humidity ratio of the supply air. Both the simulated and actual measured relative humidities showed a value between 70% and 73% during the operating period. It was difficult to determine the simulated or actual measured space humidity ratio or relative humidity during the off-period because of the migration of moisture into the space air from the external sources.
5. Both the measured and simulated surface temperatures of the partition wall dropped suddenly during the cool-down period. This is mainly due to the drop in space air temperature and the need for latent heat of vaporization. The surface temperature of the partition wall rose sharply after the air system was turned off. This is because of the sudden rise in the space air temperature.

   As soon as the surface temperature of the partition wall was lower than its value at the time just before the air system was turned on, a space sensible cooling load existed due to the heat transfer from the building structure to the space air because of the heat storage inside the building structure.
6. The measured air temperature adjacent to the surface temperature of the partition wall was about 0.2°C (0.36°F) lower than the surface temperature of the partition wall during the operating period. It is about 0.2°C (0.36°F) higher than the surface temperature during the off-period.
7. During the simulation, an increase of the mean convective mass transfer coefficient would cause the following results:

- a drop in the surface temperature of the building structure because of the need for latent heat of vaporization;
- a significant drop in the temperature difference between the surface temperature and space air;
- a significant drop in space temperature;
- a considerable decrease in the space sensible cooling load; and
- a significant increase in space latent load and total space cooling load.

8. During the simulation, an increase in the mean convective heat transfer coefficient has similar results as the increase in the convective mass transfer coefficient.
9. During the simulation, an increase in the energy of electric light downward would cause:

- a corresponding increase in the space cooling load;
- an increase in the surface temperature of the building structure and the space air; and
- an increase in the temperature difference between the surface of the building structure and the space air.

ACKNOWLEDGMENTS

The author wishes to thank Hong Kong Polytechnic, Associated Consulting Engineers, and Hong Kong Land Ltd. for supporting this study. He also wishes to express his sincere thanks to S.K. Wang for the valuable contributions to this paper. Thanks are also due to Stephen Chan, K.F. Chan, Peter Cheung, W.C. Yip, and T.L. Lau for their kind assistance in site surveys and tests. The author also expresses his thanks to Colin Chan, C.W. Au, and Elsie Wong for preparing the manuscript.

NOMENCLATURE

A = area, m^2 (ft^2)
C = specific heat, J/kg·K or kJ/kg·K (Btu/lb·°F)
c_{pa} = specific heat of moist air at constant pressure, J/kg·K or kJ/kg·K (Btu/lb·°F)
D_{lv} = mass diffusivity of liquid and vapor, m^2/s (ft^2/s)
E_c = convective heat transfer from the equipment, W (Btu/h)
E_{da} = heat released from the data acquisition unit, W (Btu/h)
E_h = electric power input to the warm air heater, W (Btu/h)
h_c = mean convective heat transfer coefficient, $W/m^2 \cdot K$ (Btu/h·ft^2·°F)
$h_{c\text{-}lp}$ = convective heat transfer coefficient of the outer surface of the upper cover of the light troffer, $W/m^2 \cdot K$ (Btu/h·ft^2·°F)
h_{fg} = latent heat of vaporization or condensation, kJ/kg (Btu/lb)
h_m = convective mass transfer coefficient, m/s (ft/s)
$h_{r\text{-}lp}$ = radiative heat transfer coefficient of the outer surface of the upper cover of the light troffer, $W/m^2 \cdot K$ (Btu/h·ft^2·°F)
k = thermal conductivity, W/m·K (Btu/h·ft·°F)
K_d = downward fraction of heat released from electric lighting
K_{leak} = leaked fraction of supply air into the ceiling plenum
K_{sc} = coefficient of structural characteristics
K_{vl} = downward fraction of visible light
L = length, m (ft); power of electric light, W (Btu/h)
L_c = convective heat transfer from light troffer, W (Btu/h)
L_w = total wattage of electric lights, W (Btu/h)
$\dot{m}$ = mass flow rate, kg/s (lb/s or lb/h)
$\dot{m}_w$ = mass flow rate of moisture transfer from the building envelope to the space air, kg/s (lb/s)
O_c = convective heat transfer from the occupant, W (Btu/h)
q = rate of heat transfer, W or kW (Btu/h)
$q_{ex\text{-}s}$ = space heat extraction rate, W or kW (Btu/h)
q_{rs} = space sensible cooling load, W or kW (Btu/h)
q_{rl} = space latent load, kW (Btu/h)
T = temperature of the building material, °C (°F)
t = time, s or h
U = internal energy, J or kJ (Btu)
$\dot{V}$ = supply volume flow rate, m^3/s or L/s (cfm)
V_c = space volume of the test chamber, m^3 (ft^3)
V_p = space volume of ceiling plenum, m^3 (ft^3)
v = velocity, m/s (fpm or ft/s)
$w_{is}^{t+\Delta t}$ = saturated humidity ratio of surface i corresponding to the surface temperature at time $t+\Delta t$, kg/kg (lb/lb)
w_r = space humidity ratio, kg/kg (lb/lb)
w_{sr} = space humidity ratio of saturated air at space temperature, kg/kg (lb/lb)
w = humidity ratio, kg/kg (lb/lb)
X = moisture content, kg/kg (lb/lb)
Δx = spacing of the section, m (ft)
α = thermal diffusivity, m^2/s (ft^2/s); coefficient of absorption
μ = degree of saturation
ρ = density of solid or moisture, kg/m^3 (lb/ft^3)
ϕ = relative humidity, %

Subscripts & Superscripts

a = air
b = building material
c = convective
g = window glass
i = number of surfaces, such as surface i; initial; inner; number of nodes
if = infiltration
j = number of surfaces of the convective heat transfer in the ceiling plenum
lp = upper cover of the light troffer
$1,2...n$ = number of nodes or surfaces
p = ceiling plenum
r = space; room; radiative
s = surface, saturated, or supply air
t = at time t
$trof$ = light troffer

BIBLIOGRAPHY

ASHRAE. 1985. *ASHRAE handbook—1985 fundamentals*, chapter 13. Atlanta: American Society of Heating, Refrigerating, and Air-Conditioning Engineers, Inc.

Cuplinskas, E.L. 1977. "Thermal response calculations by the finite difference method." *ASHRAE Transactions*, Vol. 83, Part 2.

Fairey, P.W., and Keresteciogiu, A.A. 1985. "Dynamic modeling of combined thermal and moisture transport in buildings: effect on cooling loads and space conditions." *ASHRAE Transactions*, Vol. 91, Part 2A.

Kimura, K.I. 1977. *Scientific basis of air conditioning*. London: Applied Science.

Krcity, F., and Black, W.Z. 1980. *Basic heat transfer*. New York: Harper & Row.

Wang, S.K.; Kwok, K.W.; and Watt, S.F. 1985. "Characteristics of a space air diffusion system in an indoor sports stadium." *ASHRAE Transactions*, Vol. 91, Part 2B.